Modeling and Control of a Low Speed Flywheel Driving System for Pulsed Load Mitigation in DC Distribution Networks

A. T. Elsayed, T. A. Youssef, *Student Members, IEEE,* and O. A. Mohammed, *Fellow, IEEE*

***Abstract*— This paper details the modeling and development of an improved controller design for a DC Flywheel Energy Storage System (FESS) driving circuit. The Driving system is based on a Bi-directional Buck-Boost converter. The modeling of this converter including the parasitic resistances for all the components was carried out. In this model, the equivalent circuit of the machine was integrated in the converter state space model for improved accuracy and controllability. The system has two operating modes; when the FESS is charging, the converter operates in the buck mode. A controller was designed to regulate the charging rate through controlling the machine's terminal voltage. In the discharging mode, the converter operates in the boost mode. A current controller takes over to control the injected current from the machine to the DC bus. The detailed design of both control loops was identified. Simulation results show the accuracy of the derived model and the enhanced performance of the FESS. Further, it is shown that the reversal of power flow direction was performed seamlessly. A hardware prototype of the converter was implemented and the effectiveness of the developed system was experimentally verified. The experimental results are in excellent agreement with the simulation.**

***Index Terms*—DC-DC converters, flywheel, pulsed load, shipboard power system.**

I. Introduction

DRIVEN by the latest developments in different engineering realms, such as superconducting bearings, frictionless, vacuum encased machinery and power electronic switching, flywheels gained much interest as a reliable energy storage element. Flywheel energy Storage System (FESS) or sometimes known as electromechanical batteries [1] have been used lately in several applications such as data centers [2], aerospace [3]-[4], shipboard power systems [5]-[6], UPS [7], electrification of rural areas [8], fast charging of electric vehicles [9] and improving renewable energy integration [10]. Flywheel Energy Storage Systems (FESS) operates in three operating modes: charge, stand-by and discharge. Since flywheels are classified as short term energy storage [11]- [12], the transition among these three modes should be performed rapidly, unlike other types of energy storage elements. In order for this process to be done seamlessly, a fast acting, flexible and reliable driving system is required. Moreover, the control loop should be designed accurately to avoid either slow action, high overshoot or steady state errors.

This work was partially supported by a grant from the Office of Naval Research. The authors are with the Energy Systems Research Laboratory, Department of Electrical and Computer Engineering, Florida International University, Miami, FL 33174 (e-mail: mohammed@fiu.edu).

Generally, flywheels can be classified according to their speed into low speed and high speed. High speed systems feature much lower weight and smaller size. However, they entail sophisticated technologies to reduce friction and their power output is limited by cost and difficulty of cooling [13]. A variety of machines have been discussed in the literature for use in low speed flywheel applications including induction machines (IM) [14]-[16], [9], and Doubly Fed Induction Machines (DFIM) [13], [17]-[21]. In [22], the control and performance of a large DFIM based flywheel was investigated. In this system, the stator was connected to the grid through a step up transformer while the machine secondary (rotor) was connected to a cycloconverter via slip rings. Thus, the existence of slip rings is acceptable in low speed flywheels while it is not in high speed ones. Consequently, brushless DC [23], homopolar inductor [24], Permanent Magnet Synchronous Machine (PMSM) [25]-[26], Axial Flux Permanent Magnet (AFPM) [27] and synchronous reluctance machines [28] are preferred in high speed flywheels.

Different DC-DC converters topologies are utilized in the control of low speed flywheel driving systems. However, these converters are utilized as a secondary intermediate stage not as the primary driver. In [29], a boost DC-DC converter with a parallel bypassing switch is used for FESS in UPS applications. The boost converter is operated in the flywheel discharging mode to increase the operating voltage range while it is bypassed during the charging mode since it (the boost converter) is uni-directional. A Dual Active Bridge (DAB) DC-DC converter is utilized to interface a low speed FESS to an HVDC link [30]. This system is used to smooth the output power profile from a wind farm. Hedlund *et al* proposed a sliding mode 4 quadrant DC-DC converter to be utilized in controlling the power flow to a flywheel power buffer in an all-electric EV driveline [31].

This paper addresses the control and performance of DC machine based flywheels in DC distribution networks. DC machines feature a rugged construction and reliable operation. Further, they can be interfaced to the DC distribution network through DC-DC converters which are simpler and more efficient than their AC/DC counterparts. The detailed modeling of a DC-DC converter based driving system for a FESS including the parasitic resistances for all elements was carried out. In this paper, the authors integrate the machine model with the converter model. Then a combined state space model was obtained for the entire system for each mode of operation. In order to validate the derived model, it is compared to another model estimated using the MATLAB/Simulink environment.

Two control loops were designed independently for each mode of operation. Improved voltage/current controllers are introduced to achieve steady operation during the charging and discharging modes.

The rest of the paper is organized as the follows; section II addresses the detailed modeling of the system, section III presents the controller design. Selection of FESS parameters is detailed in section IV. Simulation results are provided and discussed in section V. The hardware implementation with the experimental results are provided in section VI. Section VII gives the conclusions.

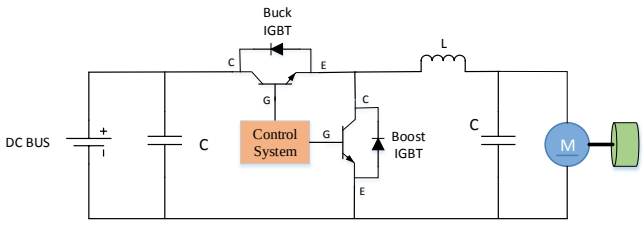

Fig. 1. Schematic diagram for flywheel driving system.

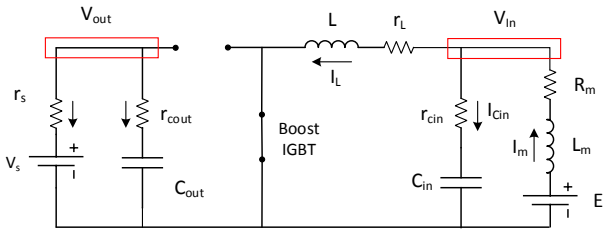

(a)

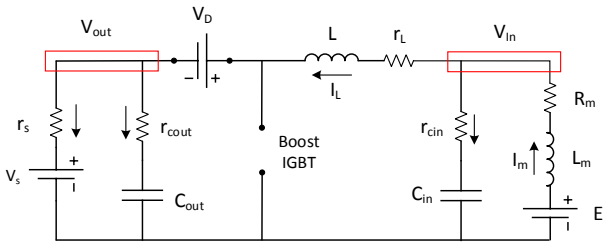

(b)

Fig.2. Equivalent circuit for the converter in boost mode during (a) ON state (b) OFF state.

II. System Modelling

The flywheel driving system is based on a DC-DC bi-directional buck-boost converter. Fig. 1 shows a schematic diagram for the system. As shown in the figure, the utilized topology features two IGBT switches; during each mode of operation, one switch is operated while the other one is disabled. Given that the DC bus voltage is higher than the machine terminal voltage over the entire operation range, the converter acts as a buck converter in the charging mode while acts as a boost during discharging. Each mode was modeled separately with its two switching states then an averaged state space model was obtained [32].

A. Discharging state (Boost mode):

In the boost mode, the source will be the machine i.e. the machine will be operated as a generator. The capacity of DC network is much larger than the FESS and the voltage of the DC bus is controlled through a large stable source (e.g. large VSC or DC generator). Thus, the DC network can be represented by a DC voltage source with a small resistance. This small impedance in the converter's output can lead to an impedance mismatch and consequently this mismatch can cause instability of the whole system due to the violation of Nyquist stability criterion [33]. In the boost mode, the control system controls the boost IGBT with a duty cycle (D) based on a reference current sent from the main distribution network controller while it disables the buck IGBT.

1) ON state

When the IGBT is in its ON state, the converter equivalent circuit tends to be as shown in Fig. 2(a). In order to obtain the most accurate model, a model of the DC machine represented by R-L-E branch is added to the converter model. The state variables are the inductor current i_L, the machine current i_m, the input capacitor voltage v_{cin} and the output capacitor voltage v_{cout}. By applying KVL and KCL, the dynamic equations of the system are derived as the following:

$$\frac{di_L(t)}{dt} = \frac{V_{In}(t) - i_L(t).r_L}{L} \quad (1)$$

Where V_{in} is the input voltage, i_L, r_L and L is the inductor current, resistance and inductance, respectively. Then by applying KCL at the input node $\left(i_{cin}(t) = i_m(t) - i_L(t)\right)$ to find V_{in} as a function of the state variables.

$$V_{In}(t) = v_{cin}(t) + i_m(t).r_{cin} - i_L(t).r_{cin} \quad (2)$$

Where r_{cin} is the input capacitor resistance. By substituting by (2) into (1) yields:

$$\frac{di_L(t)}{dt} = -\frac{1}{L}.[r_{cin} + r_L].i_L(t) + \frac{r_{cin}}{L} i_m(t) + \frac{1}{L}.V_{cin}(t) \quad (3)$$

The derivative of the machine current i_m can be evaluated as:

$$L_m \frac{di_m(t)}{dt} = E - V_{In}(t) - r_m.i_m(t) \quad (4)$$

Where L_m and r_m are the machine equivalent inductance and resistance, respectively. Similarly, by substituting from (2) into (4) and rearranging equation terms yields:

$$\frac{di_m(t)}{dt} = \frac{r_{cin}}{L_m}.i_L(t) - \frac{1}{L_m}.(r_{cin} + r_m).i_m(t) - \frac{1}{L_m}V_{cin}(t) + \frac{1}{L_m}E \quad (5)$$

The derivative of the input capacitor voltage can be expressed as:

$$\frac{dv_{cin}(t)}{dt} = -\frac{1}{C_{in}}.i_L(t) + \frac{1}{C_{in}}.i_m(t) \quad (6)$$

Where the capacitance of the input capacitor is C_{in}. In order to get V_{out} as a function of the state variables, apply KCL at V_{out} node:

$$V_{out} = V_{cout}.\frac{r_s}{(r_s + r_{cout})} + V_s.\frac{r_{cout}}{(r_s + r_{cout})} \quad (7)$$

Where V_s, r_s are the voltage and equivalent resistance of the voltage source representing the DC bus, r_{cout} is the resistance of the output capacitor. The derivative of the output capacitor voltage can be given by:

$$\frac{dv_{cout}(t)}{dt} = -\frac{1}{C_{out}.\ (r_s+r_{cout})}.V_{cout} + \frac{1}{C_{out}.\ (r_s+r_{cout})}.V_s \qquad (8)$$

Where C_{out} is the capacitance of the output capacitor. By using (3), (5), (6) and (8) to formulate the state space model as in (9) and writing it in the matrix form, results in (10) in the bottom of the next page. It should be noted here that the output equation is not used because the controlled variables are state variables [34].

$$\frac{dx(t)}{dt} = A_{on}x(t) + B_{on}.u(t) \qquad (9)$$

2) OFF state

Fig. 2(b) shows the equivalent circuit of the converter during the off state. In this case the anti-parallel diode with the buck IGBT will be forward biased. In this case the derivative of the inductor current can be calculated as the following:

$$\frac{di_L(t)}{dt} = \frac{V_{In}(t) - i_L(t).r_L - V_{out}(t) - V_D}{L} \qquad (11)$$

By applying KCL to the output node to express V_{out} as a function of state variables, yields (12):

$$V_{out} = i_L.\frac{(r_s\ .\ r_{cout})}{(r_s+r_{cout})} + V_{cout}.\frac{r_s}{(r_s+r_{cout})} + V_s.\frac{r_{cout}}{(r_s+r_{cout})} \qquad (12)$$

By substituting from (2) and (12) into (11), the derivative of the inductor current can be re-written as in (13).

$$\frac{di_L}{dt} = -\frac{1}{L}.\left[r_{cin} + r_L + \frac{(r_s\ .\ r_{cout})}{(r_s+r_{cout})}\right].i_L + \frac{r_{cin}}{L}i_m + \frac{1}{L}.V_{cin} - \frac{r_s}{L.(r_s+r_{cout})}.V_{cout} - \frac{r_{cout}}{L.(r_s+r_{cout})}.V_s \qquad (13)$$

Using a similar approach, the state space model for the converter in the OFF state can be written as shown in (14) shown at the bottom of this page. An averaged state space model is obtained by multiplying each state by its corresponding duty cycle.

$$A = A_{on}.D + A_{off}.(1-D) \qquad (15)$$

$$B = B_{on}.D + B_{off}.(1-D) \qquad (16)$$

After averaging, the system is perturbed around a steady state operation point, then linearized by neglecting second order terms. By applying Laplace transformation, the steady-state operating point can be obtained by (17).

$$X = -A^{-1}.B.U \qquad (17)$$

Given that U is the input vector, the solutions of the state variables are given by (18), then the transfer function of the duty cycle to each state variable can be obtained. In this case, the control loop of the boost converter mode will be controlling the injected current to the DC bus to fulfill the pulsed load required energy. Therefore, the important transfer function is the duty cycle-inductor current. This transfer function will be used for the accurate design and tuning of the PI controller.

$$\hat{x} = (SI - A)^{-1}.\left[(A_{on} - A_{off}).X - (B_{on} - B_{off}).U\right].\hat{d} \qquad (18)$$

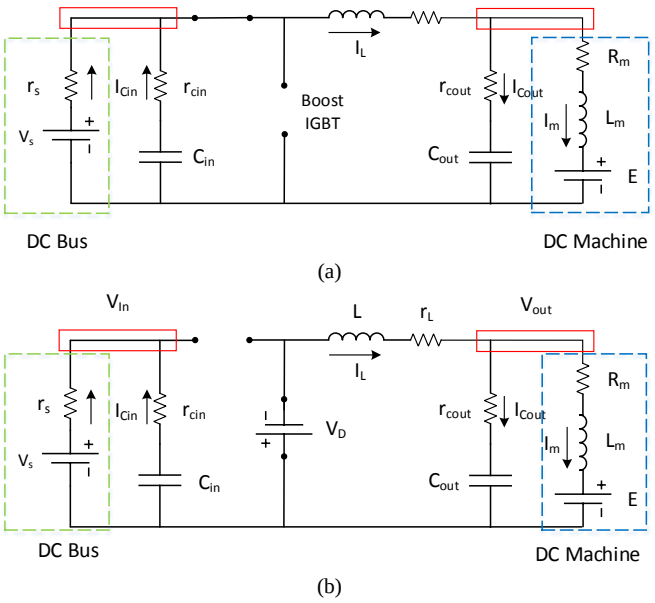

Fig.3. Equivalent circuit for the converter in buck mode during (a) ON state (b) OFF state.

B. Charging state (Buck mode):

The converter will be operated in this mode during off the pulse (the pulsed load is not energized), so there's excess energy in the system to charge the flywheel. The power flow direction will be reversed to be from the DC network to the FESS. In this mode, the DC machine is working as a motor, in contrast to the boost mode where the machine was working as

$$\frac{d}{dt}\begin{bmatrix} i_L(t) \\ i_m(t) \\ v_{cin}(t) \\ v_{cout}(t) \end{bmatrix} = \begin{bmatrix} -\frac{1}{L}.[r_{cin}+r_L] & \frac{r_{cin}}{L} & \frac{1}{L} & 0 \\ \frac{r_{cin}}{L_m} & -\frac{1}{L_m}.(r_{cin}+r_m) & -\frac{1}{L_m} & 0 \\ -\frac{1}{C_{in}} & \frac{1}{C_{in}} & 0 & 0 \\ 0 & 0 & 0 & -\frac{1}{C_{out}.\ (r_s+r_{cout})} \end{bmatrix}.\begin{bmatrix} i_L(t) \\ i_m(t) \\ v_{cin}(t) \\ v_{cout}(t) \end{bmatrix} + \begin{bmatrix} 0 & 0 & 0 \\ 0 & \frac{1}{L_m} & 0 \\ 0 & 0 & 0 \\ \frac{1}{C_{out}.\ (r_s+r_{cout})} & 0 & 0 \end{bmatrix}.\begin{bmatrix} V_s \\ E \\ V_D \end{bmatrix} \qquad (10)$$

$$\frac{d}{dt}\begin{bmatrix} i_L(t) \\ i_m(t) \\ v_{cin}(t) \\ v_{cout}(t) \end{bmatrix} = \begin{bmatrix} -\frac{1}{L}.\left[r_{cin}+r_L+\frac{(r_s\ .\ r_{cout})}{(r_s+r_{cout})}\right] & \frac{r_{cin}}{L} & \frac{1}{L} & -\frac{r_s}{L.(r_s+r_{cout})} \\ \frac{r_{cin}}{L_m} & -\frac{1}{L_m}.(r_{cin}+r_m) & -\frac{1}{L_m} & 0 \\ -\frac{1}{C_{in}} & \frac{1}{C_{in}} & 0 & 0 \\ \frac{r_s}{C_{out}.\ (r_s+r_{cout})} & 0 & 0 & -\frac{1}{C_{out}.\ (r_s+r_{cout})} \end{bmatrix}.\begin{bmatrix} i_L(t) \\ i_m(t) \\ v_{cin}(t) \\ v_{cout}(t) \end{bmatrix} + \begin{bmatrix} -\frac{r_{cout}}{L.(r_s+r_{cout})} & 0 & -\frac{1}{L} \\ 0 & \frac{1}{L_m} & 0 \\ 0 & 0 & 0 \\ \frac{1}{C_{out}.\ (r_s+r_{cout})} & 0 & 0 \end{bmatrix}.\begin{bmatrix} V_s \\ E \\ V_D \end{bmatrix} \qquad (14)$$

a generator. Figs. 3(a) and 3(b) show the converter equivalent circuits in both IGBT states. By using a similar procedure to the one used for the boost mode, the dynamic equations of the buck converter are determined during ON and OFF states and given in (19) and (20), respectively. For more clarity, both equations are listed in the bottom of the next page.

The transfer functions of the duty cycle to each state variable are determined, however the controller in the buck mode will be controlling the machine terminal voltage to control the charging rate. Thus, the transfer function of the duty cycle to the output capacitor voltage is used to design the PI control loop for the buck mode.

TABLE I
MACHINE PARAMETERS

Arm. Voltage	100 V
Arm. Current	19 A
Field Voltage	100 V
Field Current	0.6 A
r_m	0.44 Ω
L_m	12.9 mH
r_f	207 Ω
Lf	115 H
Speed	1750 rpm

TABLE II
CONVERTER PARAMETERS

DC Bus Voltage	325
r_s	0.01 Ω
C_{out}	1200 µF
r_{cout}	0.008 Ω
L	12.7mH
r_L	0.125 Ω
C_{in}	1200 µF
r_{cin}	0.008 Ω
V_D	1.75 V

C. Model Validation

Before proceeding to the controller design based on the obtained transfer functions, it is important to validate those functions. The frequency response of the determined converter model is plotted using Matlab and compared to an estimated transfer function using the approach introduced in [35]. This approach is based on building an accurate converter model in Matlab/Simulink environment. The duty cycle is then perturbed around a set point. For more details please refer to [35]. The calculations were carried out using machine and converter parameters listed in Tables I and II, respectively. The frequency responses for the determined (analytical) and estimated (simulation) transfer functions are shown in Fig. 4.

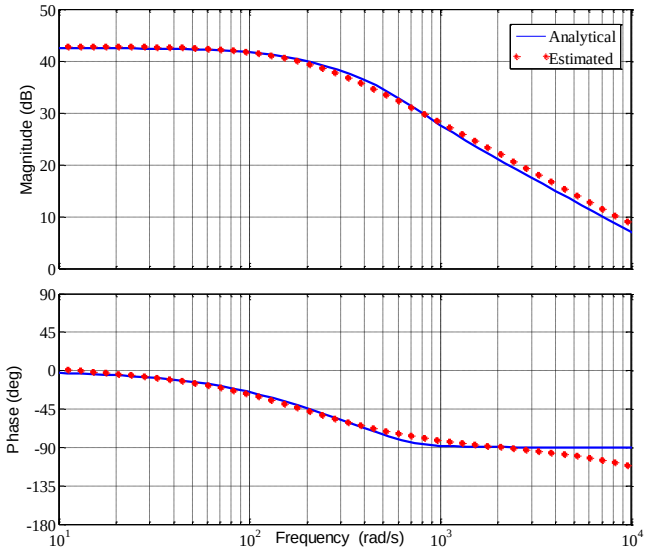

Fig.4. Frequency response of the duty cycle to inductor current transfer function for the boost converter.

III. CONTROLLER DESIGN

Two PI control loops were designed, one for each operation mode. Switching between both controllers is performed through the main supervisory controller of the distribution network based on its needs. The main purpose is to utilize the available energy in the FESS to fill the energy gap caused by the pulsed load and prevent any voltage fluctuations. The controller of the buck mode is designed to control the charging rate through the control of the machine voltage. It is known that the DC machine can withdraw high current during the starting until the motor rotation can build up the counter emf. For this reason, a constant voltage reference can't be used, rather, a soft starting approach was utilized. The controller generates an internal ramping up voltage reference. One should keep in mind that the duration of

$$\frac{d}{dt}\begin{bmatrix} i_L(t) \\ i_m(t) \\ v_{cin}(t) \\ v_{cout}(t) \end{bmatrix} = \begin{bmatrix} -\frac{1}{L}.\left[\frac{(r_s.r_{cin})}{(r_s+r_{cin})}+r_{cout}+r_L\right] & \frac{r_{cout}}{L} & \frac{r_s}{L.(r_s+r_{cin})} & -\frac{1}{L} \\ \frac{r_{cout}}{L_m} & -\frac{1}{L_m}.(r_{cout}+r_m) & 0 & \frac{1}{L_m} \\ \frac{r_s}{C_{in}.(r_s+r_{cin})} & 0 & -\frac{1}{C_{in}.(r_s+r_{cin})} & 0 \\ \frac{1}{C_{out}} & -\frac{1}{C_{out}} & 0 & 0 \end{bmatrix}.\begin{bmatrix} i_L(t) \\ i_m(t) \\ v_{cin}(t) \\ v_{cout}(t) \end{bmatrix} + \begin{bmatrix} \frac{r_{cin}}{L.(r_s+r_{cin})} & 0 & 0 \\ 0 & -\frac{1}{L_m} & 0 \\ -\frac{1}{C_{in}.(r_s+r_{cin})} & 0 & 0 \end{bmatrix}.\begin{bmatrix} V_s \\ E \\ V_D \end{bmatrix} \quad (19)$$

$$\frac{d}{dt}\begin{bmatrix} i_L(t) \\ i_m(t) \\ v_{cin}(t) \\ v_{cout}(t) \end{bmatrix} = \begin{bmatrix} -\frac{1}{L}.[r_{cout}+r_L] & \frac{r_{cout}}{L} & 0 & -\frac{1}{L} \\ \frac{r_{cout}}{L_m} & -\frac{1}{L_m}.(r_{cout}+r_m) & 0 & \frac{1}{L_m} \\ 0 & 0 & \frac{1}{C_{in}.(r_s+r_{cin})} & 0 \\ \frac{1}{C_{out}} & -\frac{1}{C_{out}} & 0 & 0 \end{bmatrix}.\begin{bmatrix} i_L(t) \\ i_m(t) \\ v_{cin}(t) \\ v_{cout}(t) \end{bmatrix} + \begin{bmatrix} 0 & 0 & -\frac{1}{L} \\ 0 & -\frac{1}{L_m} & 0 \\ \frac{1}{C_{in}.(r_s+r_{cin})} & 0 & 0 \end{bmatrix}.\begin{bmatrix} V_s \\ E \\ V_D \end{bmatrix} \quad (20)$$

the pulsed load is unknown, consequently the State of Charge (SoC) of the FESS at the end of a given discharging cycle is unknown. Since, the SoC is directly dependent on the machine speed, the machine speed and voltage are not known at the end of the pulsed load period as well. To assure a stable operation over a wide range of pulses, it is mandatory that the controller picks the last voltage value before switching to the buck mode (charging). Then the controller generates the ramping voltage reference starting from this value and ending at the full speed of the machine (full SoC). This approach allows the utilization of a very wide speed range of the machine which can be an advantage over the DFIMs. Since the operation speed range of the DFIM is limited by the allowed slip which is typically within ±15% [22] to ±30% [13].

A block diagram showing the controller design is given in Fig. 5. There are two independent Proportional Integral loops for the buck/boost modes controlling the charging and discharging of the flywheel, respectively. The transfer function for the buck mode controller is C_{buck} and C_{boost} for the boost mode controller. The gains of the two PI controllers are listed in Table III. It should be emphasized here that when the FESS is operating in a certain mode, the other IGBT should be turned off. For example, if the machine is charging, the buck mode controller is activated and the buck IGBT is working (please refer to Fig.1). Hence, the boost IGBT should be kept off and vice versa. A simple interlocking logic circuit is provided for this function. Moreover, this design is prepared to be suitable for hardware and practical implementation. An input is provided to disable the converter and turn off both switches in case of an emergency or fault. One of the merits of this controller is its simplicity with avoiding heavy computations so it can be easily implemented on any microcontroller or FPGA chip.

As mentioned previously, the converter in boost mode works in current control to control the injected current into the DC bus. The reference current (I_{ref}) is calculated and passed from an outer control loop which is typically resolved by a slower controller [9], [36]. This paper focusses on the design of the inner control loops, while the details of the outer control ones are beyond the scope of this work.

At this point, the stability of the system after adding the controller is still a concern. In order to guarantee the safe operation, the stability of the system in both operation modes shall be investigated. The root locii for the system in the boost and buck modes are traced as depicted in Fig. 6 (a) & (b), respectively. It can be seen that the poles are in the left hand side plane which implies the stable operation of the system.

IV. FESS Parameters Selection

The previous sections covered the modelling, design and control of the FESS. This section discusses the selection of the FESS speed and rate of charge to meet the requirements of a certain pulsed load. In this work, the authors are presenting a simple formula to select the optimum speed for the flywheel based on the pulsed load parameters. Flywheel speed selection is very crucial since overestimating the speed may involve unnecessary expenses and design complications. On the other hand, underestimating the speed may cause premature

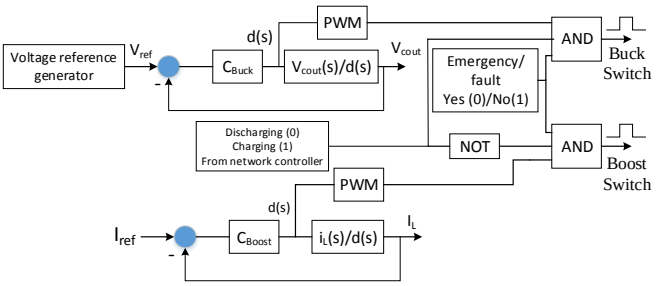

Fig.5. Block diagram for the FESS controller.

TABLE III
PI CONTROLLERS' PARAMETERS

	K_p	K_i
Buck Converter	9.75	29
Boost Converter	0.75	30.45

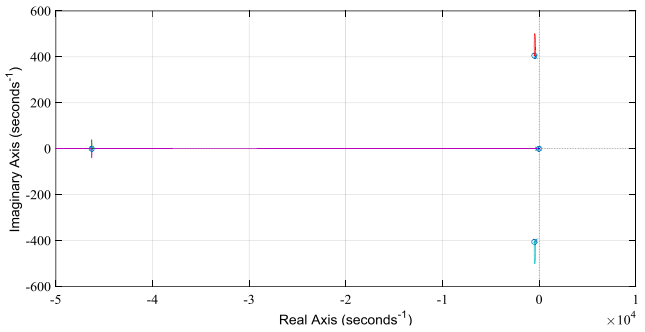

(a)

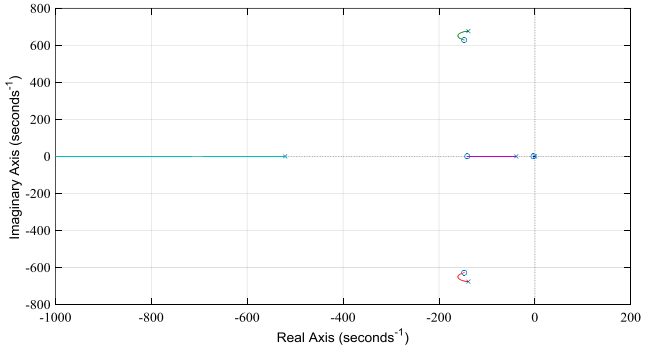

(b)

Fig.6. Root locus for the systems in (a) Boost mode (b) Buck mode.

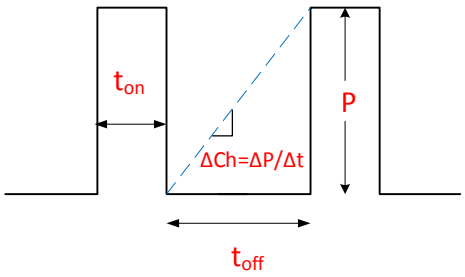

Fig.7. Generic pulsed load profile.

discharging of the flywheel and energy insufficiency to mitigate the pulsed load.

Given the generic pulsed load profile shown in Fig. 7, the amplitude of the pulse power is P, the period for the pulsed is t_{on} and the span between any two consecutive pulses is (t_{off}). It is required to calculate the minimum safe speed of the flywheel to mitigate such a load. The stored energy in the flywheel is:

$$E_{fw}=\frac{1}{2}.\mathrm{J}.\omega_{fw}^2 \tag{21}$$

Where ω_{fw} and J are the flywheel speed and moment of inertia, respectively. The amount of energy needed to mitigate a pulsed load (area under the curve) as shown is:

$$E_{Pul}=(1/\eta_{dis}).\mathrm{P}.t_{on} \tag{22}$$

Where η_{dis} is the discharging efficiency. One of the disadvantages of the flywheel is the high self-discharging rate (σ), so it will be considered in any calculations. It is worthy to mention that the self-discharge rate is dependent on the mechanical friction and type of the used bearings. This is the reason why magnetic bearing is preferred with high speed machines. With equating both energies, yield:

$$(1-\sigma).\frac{1}{2}.\mathrm{J}.\omega_{fw}^2=(1/\eta_{dis}).\mathrm{P}.t_{on} \tag{23}$$

Then the minimum flywheel speed can be calculated as:

$$\omega_{fw}=\sqrt{\frac{2.\mathrm{P}.t_{on}}{\eta_{dis}.J.(1-\sigma)}} \tag{24}$$

It is required to completely charge the flywheel at the instance of the pulse. i.e. when the pulse starts the flywheel is at 100% SoC. In order to achieve this a rate of charging, acceleration (Δ_{ch}) should be selected and embedded in the controller design. The amount of energy injected to the flywheel during t_{off} is given as:

$$E_{fw}=\frac{1}{2}.\mathrm{J}.(\omega_{fw}^2-\omega_0^2).\eta_{ch} \tag{25}$$

Where ω_0 is the flywheel speed before the acceleration (at the end of the previous pulse) and η_{ch} is the charging efficiency. Thus, the machine should be accelerated with this rate:

$$\Delta_{ch}=\frac{\omega_{fw}}{t_{off}}=\left(\frac{1}{t_{off}}\right).\sqrt{\frac{2.\mathrm{P}.t_{on}}{\eta_{ch}.J}+\omega_0^2} \tag{26}$$

In the case of random (non-uniform) pulsed loads, it is possible to change the charging rate dynamically based on the changed parameters and characteristics of the pulsed load profile. It is important to select the adequate charging rate for the flywheel to avoid premature occurrence of the pulse at early point where the flywheel is not completely charged. While, charging the flywheel with high rate (quickly) can cause unnecessary high currents which can cause fluctuations.

V. Case Studies and Discussion

A model for a DC distribution network with a pulsed load and the proposed FESS is built in Matlab/Simulink environment. The flywheel inertia (*J*) is taken as 0.75 kg.m^2. For more realistic testing, the performance of the FESS is investigated through two case studies. In the first, a purely square wave pulsed load is used while in the second case, a distorted one is applied.

A. Case I: Purely Square Wave Pulsed Load

The simulation results are shown in Fig. 8, the pulsed load profile is as shown in Fig. 8 (b). This pulse load can be either an Electromagnetic gun or Integrated Fight Through Power (IFTP) system [5]. Also, a large number of electric vehicles requesting fast charging or large cranes can represent a pulsed load. In this case, the duty cycle of the pulsed load is variable (i.e. non-uniform pulsed load profile) and its amplitude is 30 A.

The injected current to/from the DC bus is shown in Fig. 8 (a). It can be seen that during the pulse, the injected current perfectly follows the pulsed shape to fulfill the energy gap and meet the pulse load requirements. This is due to the fast yet stable response of the controller. The injected current is steady around the 30 A level which is the amplitude of the pulse.

When the Pulsed load is off the machine charges which is denoted by a negative current in Fig. 8(a). The machine terminal voltage and speed are shown in Figs. 8(d) and (f), respectively. It can be seen that the machine is accelerating smoothly during charging and then de-accelerates during the load indicating losing charge. Because of the non-uniformity of the pulse load profile, at some points, the span between any two consequent pulses is very short. Thus, the next pulse occurs while the FESS is not completely charged. The FESS can flexibly react to this situation and switch seamlessly from charging to discharging without any interruptions. Minor spikes are detected in the machine voltage during charging, this is because the higher current withdrawn during the build-up of the counter emf. This is reflected as fluctuations in the DC bus voltage. However, these fluctuations are less than 0.5 % which is acceptable by the standards [37]-[39]. On the other hand, there's no fluctuations during the pulse, which indicates complete mitigation for the pulsed load. The armature current is shown in Fig. 8(c), which is a reverse of the current shown in Fig. 8(a).

B. Case II: Distorted Pulsed Load

Although most of the pulsed loads have a nearly pure square waveform [40]-[1], but in some real world scenarios, they may exhibit a distorted shape. In order to achieve a broader investigation for the FESS performance, a pulsed load with a distorted waveform is simulated and applied to the system. The results are depicted in Fig. 9, the load profile is shown in Fig. 9(a). The machine current and speed are shown in Figs. 9 (b) &(c), respectively. From Fig. 9 (d), it can be seen that the FESS is still compensating the load efficiently with preventing any fluctuations on the DC bus voltage.

VI. Hardware Implementation and Experimental Results

The Developed design for the FESS was implemented as shown in Fig. 10. The current flowing in the system is measured at four points I1, I2, I3 and I4. The DC bus and machine voltages are measured. The machine is coupled to a 12 in. diameter steel disc as the rotating mass. Fig. 11 shows a block diagram for the implemented hardware setup. The converter

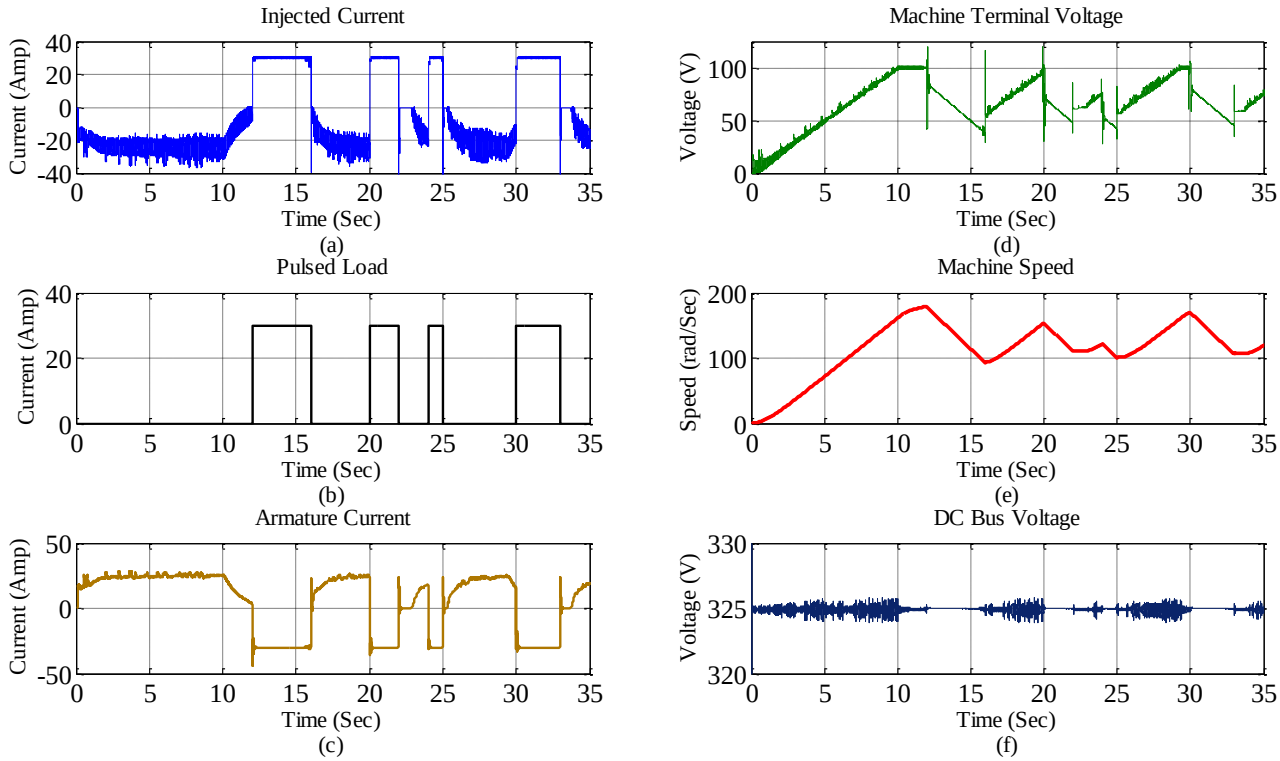

Fig.8. FESS operation under pulsed load.

was designed and implemented in a modular manner for ease of assembly, diagnostics and maintenance. Two fast IGBT modules with anti-parallel diodes were used, the module part number is HGTG30N60C3D. The converter was implemented in two main separable parts. The first one is the main board to carry the power components. The second comprises the control, protection and the driving circuits. Different protection functions were provided to disable the IGBT gate signals and protect the system. These functions are loss of field, over voltage, over current and IGBT driver error. 4 LEDS are used to indicate the type of fault. A varistor was connected at the converter side connected to the machine terminals to protect the machine against overvoltages. The system control was implemented using dSPACE 1104. The switching frequency was 10 kHz.

In order to examine the effectiveness of the developed system, the system will be tested under a heavy pulsed load (11.5 Amps at 318 DCV). Fig. 12 depicts the system results without the flywheel. It can be seen that under the pulsed load, the bus voltage drops to around 297.5 V (93.5%) violating the limits specified by the standards (indicated by red dashed lines). It should be noted that the allowed range for voltage variation is ±5%. This can result in disconnection of critical loads or underperformance of some other loads in the system.

The FESS is connected to mitigate the effect of the pulsed load and share the load with the supply to fill the energy deficit. The experiment was performed under the same load conditions. The experimental results are depicted in Fig. 13. It can be seen that the pulsed load current is shared between the DC bus and the FESS. Thus, the FESS clipped the pulsed load current to

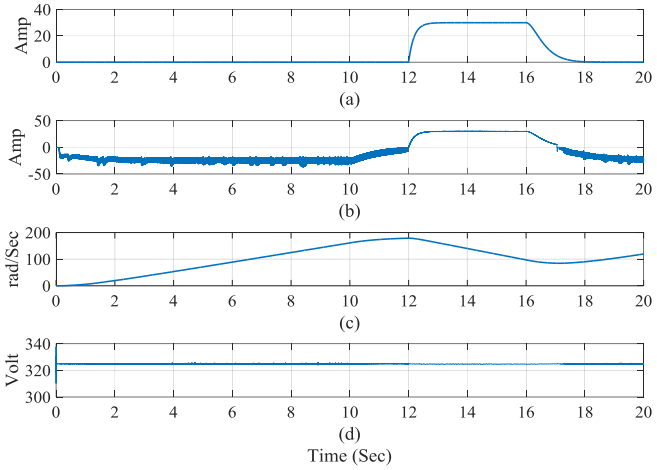

Fig.9. FESS performance under distorted pulsed load (a) Load current (b) Machine current (c) Machine speed (d) Bus voltage.

limit the loading on the DC bus and maintain the voltage. Also, the machine charging current is shown on the bus current but with reversed sign as the current direction is reversed. The pulsed load current (I_3) is the algebraic sum of the DC bus current (I_1) and the machine current (I_2). Since, the voltage at the machine side is less than the DC bus side (one third of the DC bus voltage), the current in the machine side of the converter is around three times that of the DC bus side i.e. ($I_4 \approx 3*I_2$).

It is shown that the machine voltage is increasing gradually indicating smooth charging of the flywheel. The charging current of the machine is increasing smoothly as well without

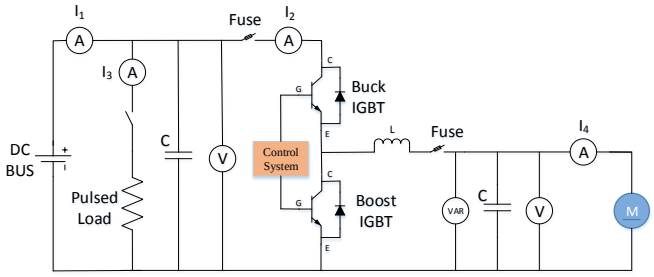

Fig.10. Hardware implementation of FESS with pulsed load.

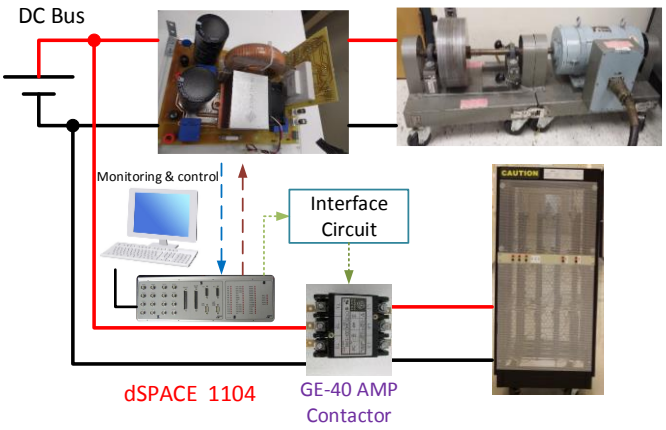

Fig.11. Experimental setup.

large spikes. Then, the voltage is constant around the reference value which is 85 Volts. Finally, the DC bus voltage is shown in the figure at the bottom. Some high frequency fluctuations are detected due to the charging and discharging of the machine and switching actions. However, the magnitude of these voltage spikes are well below allowed limits by the standards (the limits are shown with the red dashed lines). Thus, the effectiveness of the developed system is proven. The effect of the pulsed load didn't propagate to the DC bus which allows adding more critical loads to the DC bus without being concerned with the impacts of the pulsed load.

VII. Conclusion

In low speed flywheels, DFI and DC machines can be used. Both are using mechanical contacts for rotor connection, which is acceptable in such applications. This paper presented an improved modeling and control method for a DC machine based low speed FESS. The DC machine can offer more advantages including lower cost, simplicity and wider speed range. This wide operation range allows more utilization of the stored kinetic energy. The machine model was integrated to the converter model. A state space model was obtained for the entire system as a single entity. The model was validated through a comparison with another estimated model. Based on the obtained model, accurate tuning of the PI controllers was achieved. An efficient performance was shown through simulation results under heavy pulsed load with non-uniform profile. The proposed design was validated through hardware setup and the experimental results were aligned with the simulation. It was shown through laboratory hardware setup that the FESS is effectively mitigating the pulsed load.

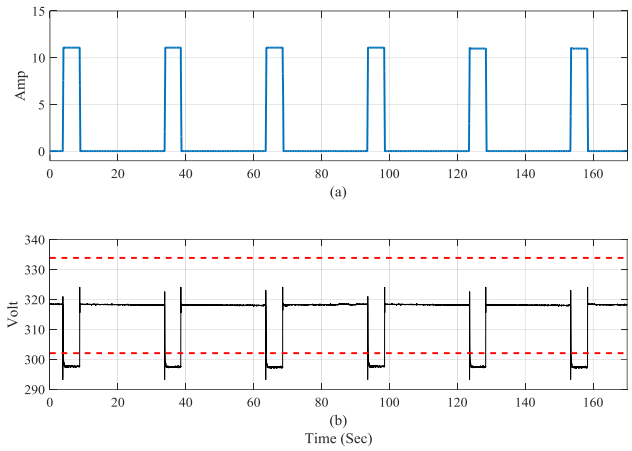

Fig.12. System performance without FESS (a) pulsed load profile (b) DC bus voltage.

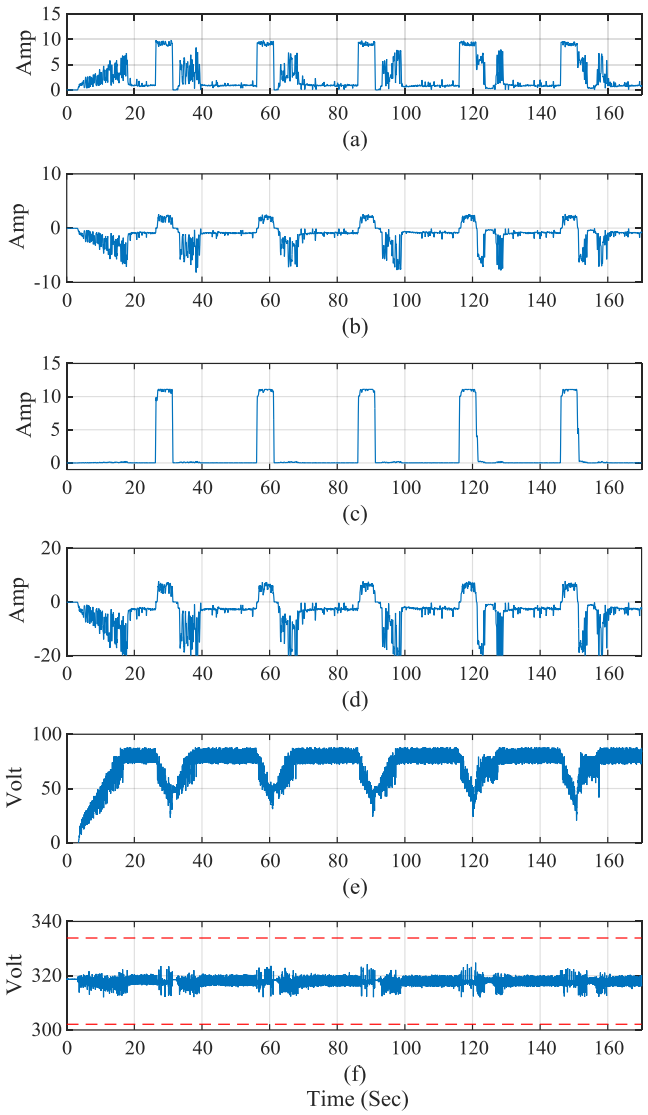

Fig.13. Experimental results showing FESS performance under pulsed load (a) Bus current (I_1). (b) Converter current-bus side (I_2). (c) Pulsed load current (I_3). (d) Converter current-machine side (I_4). (e) Machine voltage. (f) Bus voltage.

REFERENCES

[1] R. Hebner, J. Beno and A. Walls, "Flywheel batteries come around again," IEEE Spectrum, vol. 39, no. 4, pp. 46–51, 2002.

[2] S. McCluer and J.-F. Christin "Comparing Data Center Batteries, Flywheels, and Ultracapacitors," Schneider Electric-Data Center Science Center, white paper No. 65, Rev. 2, 2011.

[3] B. H. Kenny, R. Jansen, P. Kascak, T. Dever, and W. Santiago, "Integrated power and attitude control with two flywheels," IEEE Transactions on Aerospace and Electronic Systems, vol.41, no.4, pp.1431,1449, Oct. 2005.

[4] B.H. Kenny, P.E. Kascak, R. Jansen, T. Dever, and W. Santiago, "Control of a high-speed flywheel system for energy storage in space applications," *IEEE Transactions on Industry Applications*, vol.41, no.4, pp.1029,1038, July-Aug. 2005.

[5] H. A. Toliyat, S. Talebi, P. McMullen, Co Huynh and A. Filatov, "Advanced high-speed flywheel energy storage systems for pulsed power applications," *IEEE Electric Ship Technologies Symposium*, PP. 379-386, 2005.

[6] J. McGroarty, J. Schmeller, R. Hockney and M. Polimeno, "Flywheel energy storage systems for electric start and an all-electric ship," IEEE Electric Ship Technologies Symposium, PP. 400-406, 2005.

[7] R. G. Lawrence, K. L. Craven, and G. D. Nichols, "Flywheel UPS," *IEEE Industry Applications Magazine*, vol.9, no.3, pp.44-50, May-June 2003.

[8] R. Okou, A. Sebitosi, M. A. Khan, P. Barendsa, and P. Pillay "Design and analysis of an electromechanical battery for rural electrification in sub-Saharan Africa," IEEE Transactions on Energy Conversion, vol. 26, no. 4, pp. 1198-1209, Dec. 2011.

[9] T. Dragicevic, S. Sucic, J.C. Vasquez, and J.M. Guerrero, "Flywheel-Based Distributed Bus Signalling Strategy for the Public Fast Charging Station," *IEEE Transactions on Smart Grid*, vol.5, no.6, pp.2825,2835, Nov. 2014.

[10] G.O. Suvire, M.G. Molina, and P.E. Mercado, "Improving the Integration of Wind Power Generation Into AC Microgrids Using Flywheel Energy Storage," *IEEE Transactions on Smart Grid*, vol.3, no.4, pp.1945,1954, Dec. 2012

[11] Bingsen Wang, and G. Venkataramanan,"Dynamic Voltage Restorer Utilizing a Matrix Converter and Flywheel Energy Storage," *IEEE Transactions on Industry Applications*, vol.45, no.1, pp.222-231, Jan.-Feb. 2009.

[12] R. Arghandeh, M. Pipattanasomporn, and S. Rahman, "Flywheel Energy Storage Systems for Ride-through Applications in a Facility Microgrid," IEEE Transactions on Smart Grid, vol.3, no.4, pp.1955-1962, Dec. 2012.

[13] L. Ran, Dawei Xiang, J.L. Kirtley, "Analysis of Electromechanical Interactions in a Flywheel System With a Doubly Fed Induction Machine," IEEE Transactions on Industry Applications, vol.47, no.3, pp.1498-1506, May-June 2011.

[14] S. Samineni, B.K. Johnson, H.L. Hess, and J.D. Law, "Modeling and analysis of a flywheel energy storage system for Voltage sag correction," IEEE Transactions on Industry Applications, vol.42, no.1, pp.42-52, Jan.-Feb. 2006.

[15] M.I. Daoud, A. Massoud, S. Ahmed, A.S. Abdel-Khalik, and A. Elserougi, "Ride-through capability enhancement of VSC-HVDC based wind farms using low speed flywheel energy storage system," 2014 Twenty-Ninth Annual IEEE Applied Power Electronics Conference and Exposition (APEC), pp.2706-2712, 16-20 March 2014.

[16] M.I. Daoud, A.S. Abdel-Khalik, A. Elserougi, S. Ahmed, and A.M. Massoud, "DC bus control of an advanced flywheel energy storage kinetic traction system for electrified railway industry," 39th Annual Conference of the IEEE Industrial Electronics Society, IECON 2013, pp.6596-6601, 10-13 Nov., 2013.

[17] A.S. Abdel-Khalik, A.A. Elserougi, A.M. Massoud, and S. Ahmed, "Fault Current Contribution of Medium Voltage Inverter and Doubly-Fed Induction-Machine-Based Flywheel Energy Storage System," IEEE Transactions on Sustainable Energy, vol.4, no.1, pp.58-67, Jan. 2013.

[18] A. Abdel-Khalik, A. Elserougi, A. Massoud, and S. Ahmed, "A power control strategy for flywheel doubly-fed induction machine storage system using artificial neural network," Electric Power Systems Research, vol 96, pp. 267-276, March 2013.

[19] D. Kairous, and R. Wamkeue, "DFIG-based fuzzy sliding-mode control of WECS with a flywheel energy storage," Electric Power Systems Research, vol 93, pp. 16-23, December 2012.

[20] J. Goncalves de Oliveira, H. Schettino, V. Gama, R. Carvalho, and H. Bernhoff, "Study on a doubly-fed flywheel machine-based driveline with an AC/DC/AC converter," IET Electrical Systems in Transportation, vol.2, no.2, pp.51-57, June 2012.

[21] I.A. Gowaid, A.A. Elserougi, A.S. Abdel-Khalik, A.M. Massoud, and S. Ahmed, "A series flywheel architecture for power levelling and mitigation of DC voltage transients in multi-terminal HVDC grids," IET Generation, Transmission & Distribution, vol.8, no.12, pp.1951-1959, Dec. 2014.

[22] H. Akagi, and H. Sato, "Control and performance of a doubly-fed induction machine intended for a flywheel energy storage system," IEEE Transactions on Power Electronics, vol.17, no.1, pp.109-116, Jan 2002.

[23] S.R. Gurumurthy, V. Agarwal, and A. Sharma, "Optimal energy harvesting from a high-speed brushless DC generator-based flywheel energy storage system," IET Electric Power Applications, vol.7, no.9, pp.693-700, November 2013.

[24] P. Tsao, M. Senesky, and S.R. Sanders, "An integrated flywheel energy storage system with homopolar inductor motor/generator and high-frequency drive," *IEEE Transactions on Industry Applications*, vol.39, no.6, pp.1710,1725, Nov.-Dec. 2003

[25] Long Zhou, and Zhi ping Qi, "Modeling and control of a flywheel energy storage system for uninterruptible power supply," International Conference on Sustainable Power Generation and Supply, 2009. SUPERGEN '09. , pp.1-6, 6-7 April 2009

[26] M. M. Flynn, P. McMullen, and O. Solis, "Saving energy using flywheels," *IEEE Industry Applications Magazine*, vol.14, no.6, pp.69-76, November-December 2008.

[27] T. D. Nguyen, K. J. Tseng, S. Zhang, and H. T. Nguyen, "A novel axial flux permanent magnet machine for flywheel energy storage system: Design and analysis," *IEEE Transactions on Industrial Electronics*, vol. 58, no. 9, pp. 3784–3794, Sep. 2011.

[28] Jae-Do Park; C. Kalev, and H.F. Hofmann, "Control of High-Speed Solid-Rotor Synchronous Reluctance Motor/Generator for Flywheel-Based Uninterruptible Power Supplies," IEEE Transactions on Industrial Electronics, vol.55, no.8, pp.3038-3046, Aug. 2008.

[29] R. S. Weissbach, G. G. Karady, and R. G. Farmer, "A combined uninterruptible power supply and dynamic voltage compensator using a flywheel energy storage system," *IEEE Transactions on Power Delivery*, vol.16, no.2, pp.265-270, Apr 2001.

[30] Raymond G. Gadelrab, Mostafa S. Hamad, Ayman S. Abdel-Khalik, Amr El Zawawi, "Wind farms-fed HVDC system power profile enhancement using solid state transformer based flywheel energy storage system," *Journal of Energy Storage*, vol. 4, pp. 145-155, Dec. 2015.

[31] Magnus Hedlund, Janaína G. Oliveira, Hans Bernhoff, "Sliding mode 4-quadrant DC-DC converter for a flywheel application," *Control Engineering Practice*, vol. 21, no. 4, pp. 473-482, Apr. 2013.

[32] R. D. Middlebrook and S. Cuk, "A general unified approach to modelling switching-converter power stages," IEEE Power Electronics Specialists Conference Record PESC, pp. 18-34, 1976.

[33] A.A.A. Radwan, and Y.A.-R.I. Mohamed, "Linear Active Stabilization of Converter-Dominated DC Microgrids," IEEE Transactions on Smart Grid, vol.3, no.1, pp.203-216, March 2012.

[34] M. C. Mira, A. Knott, O. C. Thomsen, and M. A. E. Andersen, "Boost converter with combined control loop for a stand-alone photovoltaic battery charge system," 2013 IEEE 14th Workshop on Control and Modeling for Power Electronics (COMPEL), pp.1-8, 23-26 June 2013.

[35] Available Online: http://www.mathworks.com/help/ident/examples/estimating-transfer-function-models-for-a-boost-converter.html.

[36] M.A. Awadallah, and B. Venkatesh,"Energy Storage in Flywheels: An Overview," *Canadian Journal of Electrical and Computer Engineering*, vol.38, no.2, pp.183-193, Spring 2015.

[37] *Department of Defense Interface Standard for shipboard systems: Electric Power, Direct Current*, MIL-STD-1399, Section 390, Oct. 1987.

[38] IEEE Recommended Practice for Electrical Installations on Shipboard," IEEE Std 45-2002, Oct. 2002.

[39] M. W. Earley, J. S. Sargent, C. D. Coache, and R. J. Roux " National electrical code handbook," Twelfth edition, NFPA, 2011.

[40] J. I. Garate, E. Ibarra, I. Martínez de Alegría, I. Kortabarria, and J.A. Araujo, "Analysis of DC–DC power supply systems for pulsed loads from green electronics perspective," *IET Power Electronics*, vol.8, no.6, pp.957-966, 2015.

[41] M. Farhadi, and O. A. Mohammed, "Performance Enhancement of Actively Controlled Hybrid DC Microgrid Incorporating Pulsed Load," *IEEE Transactions on Industry Applications*, vol.51, no.5, pp.3570-3578, Sept.-Oct. 2015

Ahmed T. Elsayed (GS'2012) received his B.Sc. and M.Sc. degrees from the Faculty of Engineering, Benha University, Egypt in 2006 and 2010, respectively. From 2006 to 2012, he was a research/teaching assistant in the Faculty of Engineering, Benha University. Currently, he is a PhD candidate and a research assistant at the Electrical and Computer Engineering Department, College of Engineering and Computing, Florida International University, Miami, Florida, USA. His current research interests include DC distribution architectures, multi-objective optimization and Flywheel energy storage.

Tarek A. Youssef was born in Cairo, Egypt. He received the B.S. and M.S. Degrees in electrical engineering from Helwan University, Cairo, Egypt. Tarek has more than 10 years' experience in communication and security field. He worked as researcher in the Université Libre de Bruxelles, Belgium. In 2012 Tarek moved to energy systems research laboratory, Florida International University. He is currently a Ph.D. candidate. His Ph.D. Topic is Co-Design of Security Aware Power System Distribution Architecture as Cyber Physical System.

His research interests include cyber physical systems, communication, Wide area measurement, smart grid security, and real time monitoring of power system. Furthermore, he also has interest in artificial intelligence and signal processing applications in the power and energy systems area.

Osama A. Mohammed (S'79, SM'84, F'94): is a Professor of Electrical Engineering and is the Director of the Energy Systems Research Laboratory at Florida International University, Miami, Florida. He received his Master and Doctoral degrees in Electrical Engineering from Virginia Tech in 1981 and 1983, respectively. He has performed research on various topics in power and energy systems in addition to computational electromagnetics and design optimization in electric machines, electric drive systems and other low frequency environments. He performed multiple research projects for several Federal agencies since 1990's dealing with; power system analysis, physics based modeling, electromagnetic signature, sensorless control, electric machinery, high frequency switching, electromagnetic Interference and ship power systems modeling and analysis. Professor Mohammed has currently active research programs in a number of these areas funded by DoD, the US Department of Energy and several industries.

Professor Mohammed is a world renowned leader in electrical energy systems and computational electromagnetics. He has published more than 400 articles in refereed journals and other IEEE refereed International conference records. He also authored a book and several book chapters. Professor Mohammed is an elected Fellow of IEEE and is an elected Fellow of the Applied Computational Electromagnetic Society. Professor Mohammed is the recipient of the prestigious IEEE Power and Energy Society Cyril Veinott electromechanical energy conversion award and the 2012 outstanding research award from Florida International University. He serves as editor of several IEEE Transactions including the IEEE Transactions on Energy Conversion, the IEEE Transactions on Smart Grid, IEEE Transactions on Industry Applications and COMPEL.